Six-Degree-of-Freedom Localization of an Untethered Magnetic Capsule Using a Single Rotating Magnetic Dipole

Katie M. Popek, Thomas Schmid, and Jake J. Abbott

***Abstract*—This paper presents a method to estimate the six-degree-of-freedom pose of a magnetic capsule, with an embedded permanent magnet and Hall-effect sensors, using a rotating dipole field. The method's convergence properties as a function of the number of distinct rotation axes of the applied field and the number of complete rotations about each axis are characterized. Across our tested workspace, the localization error was 4.9 ± 2.7 mm and 3.3 ± 1.7 degrees (mean $\pm$ standard deviation). We experimentally demonstrate this is sufficient for propulsion of a screw-type magnetic capsule through a lumen using a single dipole to both propel and localize the capsule.**

***Index Terms*—Localization, medical robots and systems.**

I. Introduction

WIRELESS capsule endoscopes are a promising diagnostic tool, providing the ability to view the entire gastrointestinal tract with minimal patient discomfort. Their effectiveness is currently limited due to their uncontrolled nature, which causes the capsule to miss regions of interest. Researchers have been investigating a variety of methods to actively propel and localize these devices to enable views of the entire gastrointestinal tract painlessly and without anesthesia [1]. Propelling capsules with magnetic fields is clinically feasible [2], and utilizing magnetic fields has the benefit of being able to propel/control [3]–[7] and localize [8]–[17] the capsule using the same technology.

Previous work from our lab characterized the use of a single rotating magnetic dipole positioned in space with a robotic manipulator to propel a screw-type magnetic capsule in a lumen from any position [6]; our experimental verification previously relied on cameras to localize the capsule. In this paper, we describe a companion localization method to estimate the six-degree-of-freedom (6-DOF) pose of a magnetic capsule with no prior location information other than the bounds of its potential workspace, using the same magnetic field that is propelling it. We then apply that estimate to propel a capsule in a lumen.

There are several previously published magnetic localization algorithms, but most rely on external magnetic sensors and are either not compatible with magnetic actuation [8]–[11] or currently have a limited workspace [16]. Methods employing internal magnetic sensors (i.e., inside the capsule) require the addition of an accelerometer [12], [13], provide less than 6-DOF information [12], [16], [17], or must manipulate the position of the external magnetic source during localization [15], [17]. Frequently, localization methods rely on complicated models of the magnetic field [13]–[15], but in certain cases, which we exploit, the external magnetic source can be modeled with the simpler point-dipole equation.

This paper presents a localization method that solves for the 6-DOF pose of a magnetic capsule while it is either stationary or in the "step-out" regime where the field is rotating too quickly for the capsule to rotate synchronously with the field. Similar methods for pose detection in rotating magnetic fields exist [14], [18], but our new method is more robust to sensor noise and data synchronization issues because it utilizes all field-sensor data independently instead of relying solely on the estimated maximum and minimum field magnitudes throughout a rotation cycle, and the entire 6-DOF pose is solved simultaneously rather than solving for position and orientation sequentially. Previous methods only rotated the field about a single axis, but we show that using additional rotation axes improves accuracy. Our improved localization method was briefly introduced in [19]. In this paper, we provide further experimental validation and analysis of the convergence properties, and we experimentally demonstrate this method's accuracy is sufficient to propel a magnetic capsule by combining the localization method and our previously published propulsion method [6].

The paper is organized as follows: Section II details our localization method. Section III describes our experimental hardware. Section IV simulates the expected results based on our method (II) and hardware (III). Section V provides experimental verification. Finally, Section VI demonstrates propulsion of a capsule using our localization method to provide position and heading feedback.

II. Localization Method

Assume that the rotating magnetic dipole (i.e., the external magnet) is positioned in space by a robotic manipulator, and

Manuscript received May 9, 2016; revised July 28, 2016; accepted August 29, 2016. Date of publication September 12, 2016; date of current version September 26, 2016. This paper was recommended for publication by Associate Editor J. Nieto and Editor C. Stachniss upon evaluation of the reviewers comments. This work was supported by the National Science Foundation under Grants 0952718 and 0654414.

K. M. Popek is with the School of Computing and the Robotics Center, University of Utah, Salt Lake City, UT 84112 USA (e-mail: katie.popek@utah.edu).

T. Schmid is with the Department of Electrical and Computer Engineering, University of Utah, Salt Lake City, UT 84112 USA (e-mail: thomas.schmid@utah.edu).

J. J. Abbott is with the Department of Mechanical Engineering and the Robotics Center, University of Utah, Salt Lake City, UT 84112 USA (e-mail: jake.abbott@utah.edu).

This paper has supplementary downloadable material available at http://ieeexplore.ieee.org, provided by the author.

Color versions of one or more of the figures in this letter are available online at http://ieeexplore.ieee.org.

Digital Object Identifier 10.1109/LRA.2016.2608421

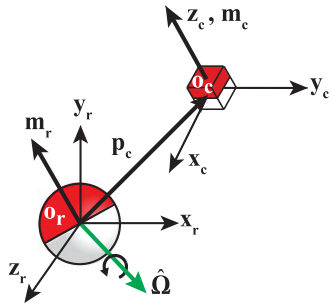

Fig. 1. Overall system setup with the robot frame origin ($\mathbf{o}_r$) at the center of the external magnetic source and the capsule frame ($\mathbf{o}_c$) at the center of the capsule's internal permanent magnet.

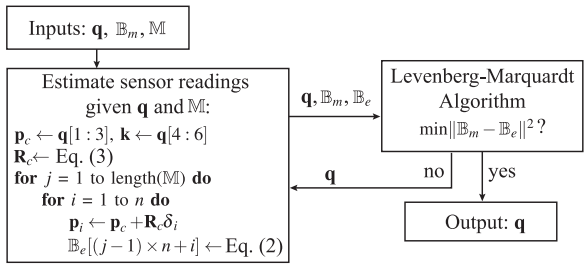

Fig. 2. A diagram depicting our localization method. $\mathbb{B}_m$ is an array of sensor measurements in one batch of data, $\mathbb{M}$ is the set of $\mathbf{m}_r$ corresponding in time to each set of n sensor measurements in $\mathbb{B}_m$, and $\mathbf{q}$ is the capsule's state, which is iteratively updated from an initial guess.

the dipole is located at the center of the robot's tool frame, $\mathbf{o}_r$, which is also our reference frame. The capsule's coordinate-frame origin, $\mathbf{o}_c$, resides at the center of the capsule's internal magnet. There exists some vector $\mathbf{p}_c$ that corresponds to the displacement between the two coordinate-frame origins as shown in Fig. 1. There also exists a rotation matrix, $\mathbf{R}_c$, that rotates the capsule's coordinate-frame to align with the robot's. By solving for the position vector, $\mathbf{p}_c$, and the rotation matrix, $\mathbf{R}_c$, the capsule's position and orientation relative to the external magnetic source is known.

The following assumptions were made in developing this method: 1) The position and orientation of the external dipole moment, $\mathbf{m}_r$, are known relative to a global frame. 2) $\mathbf{m}_r$ is rotated about an axis $\hat{\mathbf{\Omega}}$ such that $\mathbf{m}_r^T \hat{\mathbf{\Omega}} = 0$ is always true (throughout this paper, we use the "hat" symbol $\hat{}$ to indicate a unit vector). 3) The capsule is free to move, but the dipole-field rotation is well above the step-out frequency, such that we can assume no net motion, and decouple the localization and propulsion of the capsule; existing state-estimation methods can be used to ensure this is true [20]. 4) The field of the external magnet can be accurately modeled by the point-dipole equation [21]:

$$\mathbf{b}(\mathbf{p}_c) = \frac{\mu_0}{4\pi||\mathbf{p}_c||^5}\left(3\mathbf{p}_c\mathbf{p}_c^T - \mathbf{I}||\mathbf{p}_c||^2\right)\mathbf{m}_r = \frac{\mu_0}{4\pi||\mathbf{p}_c||^5}\mathbf{B}\mathbf{m}_r \tag{1}$$

where μ_0 is the permeability of free space, $\mathbf{I}$ is the identity matrix, and $\mathbf{B} = \mathbf{B}(\mathbf{p}_c)$ is a symmetric matrix. In our setup, we use a spherical permanent magnet as the external source, which is accurately approximated by (1); errors introduced by other external-magnet geometries are quantified in [22].

Consider a set of n magnetic sensors embedded inside the capsule, each with a constant known position offset, $\boldsymbol{\delta}_i$, and orientation, $\mathbf{s}_i$, expressed in the capsule frame. The position vector, $\mathbf{p}_i$, describing the position of sensor i in the robot frame, is $\mathbf{p}_i = \mathbf{p}_c + \mathbf{R}_c\boldsymbol{\delta}_i$. The scalar magnetic-field projection measured at each sensor is found by projecting (1) onto the measuring axis of the sensor, $\mathbf{s}_i$:

$$b_i(\mathbf{p}_i) = \mathbf{s}_i^T\mathbf{R}_c^T\frac{\mu_0}{4\pi||\mathbf{p}_i||^5}\left(3\mathbf{p}_i\mathbf{p}_i^T - \mathbf{I}||\mathbf{p}_i||^2\right)\mathbf{m}_r \tag{2}$$

From [23], a rotation matrix can be reduced to three variables using its exponential form:

$$\mathbf{R}_c = e^{\mathbf{S}\{\mathbf{k}\}} \tag{3}$$

where $\mathbf{S}\{\mathbf{k}\}$ is a skew-symmetric matrix packing of the angle-axis representation $\mathbf{k} = \hat{\mathbf{k}}\theta$.

The capsule's full 6-DOF pose is represented by $\mathbf{q} = \left[\mathbf{p}_c^T\ \mathbf{k}^T\right]^T$. We use the nonlinear least-squares Levenberg-Marquardt algorithm [24] to estimate the capsule pose by minimizing the cost function $c = ||\mathbb{B}_m - \mathbb{B}_e||^2$, where $\mathbb{B}_m$ is an array of the measured magnetic field readings, and $\mathbb{B}_e$ is an array of the magnetic field readings estimated by (2). A diagram of our method is shown in Fig. 2; the capsule's state is iteratively manipulated using the Levenberg-Marquardt algorithm until a minimum c is found. We use a numerically approximated Jacobian in our testing, both in MATLAB (calculated by default when using *lsqnonlin()*) and in C++ with the NonLinearOptimization module of the Eigen library [25].

A static magnetic field does not provide enough information to uniquely determine the capsule's pose; additional data must be obtained by either translating or rotating the external dipole. This method can be utilized in applications with any changing applied magnetic field that can be modeled by (1), however, this paper deals exclusively with a rotating dipole field to be consistent with our previous propulsion method [6]. Using a dipole field that rotates about only one axis will result in limited information in certain configurations; for example, if the dipole is located along the axis of rotation of the capsule, the field's magnitude along the capsule's axis may remain constant throughout the rotation of the dipole. As detailed in [18], there also exist multiple poses in the workspace that produce the same magnetic field if the dipole is rotated about only one axis. Because we do not have prior knowledge of the capsule's pose, the choice of a single $\hat{\mathbf{\Omega}}$ for robust localization across the entire workspace is not feasible. To span the workspace, we chose to populate $\mathbb{B}_m$ by rotating the dipole source about its three coordinate-frame axes $(\mathbf{x}_r, \mathbf{y}_r, \mathbf{z}_r)$ successively for a single dataset. The number of distinct $\hat{\mathbf{\Omega}}$ and the amount of data needed for the algorithm to converge is explored in Section V.

III. Experimental Hardware

A. Magnetic Dipole Source

The experimental setup is shown in Fig. 3(a). The spherical-actuator-magnet manipulator (SAMM) [26] is used as the external dipole. The device provides a singularity-free method for controlling a spherical permanent magnet's dipole orientation

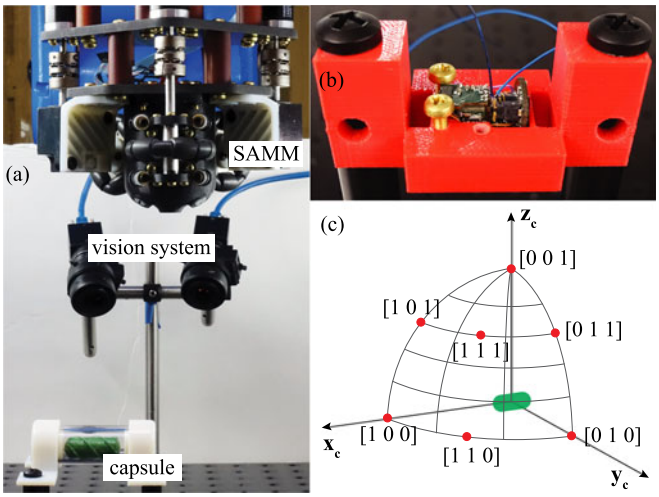

Fig. 3. (a) The experimental setup with the SAMM mounted on the end-effector of a 6-DOF robotic arm, the stereo vision system used for ground truth, and our capsule constrained to a lumen where it is free to rotate about its long axis, but not translate. (b) The test fixture used to rigidly mount the sensor array. (c) Experimentally tested positions of the dipole are denoted by red dots and their corresponding direction vectors in the capsule's frame. The distance to the capsule was varied.

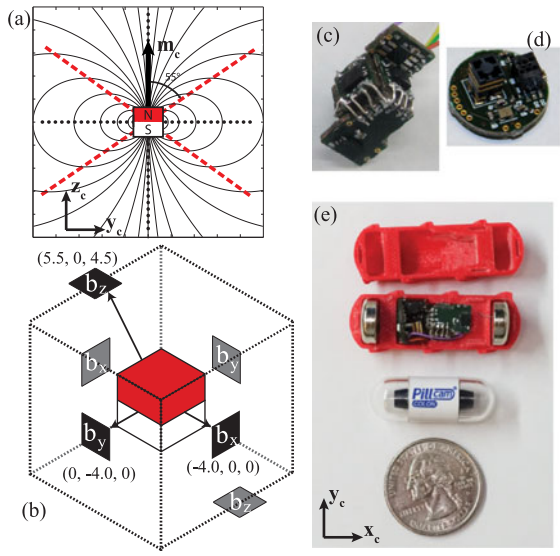

Fig. 4. (a) A magnetic dipole field has regions where the field vector points in a single cardinal direction, denoted by dashed/dotted lines. Place $\mathbf{b_z}$ sensors along the red dashed lines and $\mathbf{b_y}$ sensors in regions denoted by the black dotted lines (with $\mathbf{b_x}$ sensors placed analogously). (b) An isometric view of our final sensor layout with each sensor labeled with its measured field direction, and its position offset in mm with respect to the center of the magnet. The gray sensors are not visible from this angle, but are located at the negative counterpart of the corresponding sensor. (c) The sensor array (i.e., the hardware implementation of (b)) surrounding a permanent magnet. (d) The communications electronics. (e) Our capsule compared to Given Imaging's colon capsule. Along with the electronics shown in (c) and (d) it contains coin cell batteries on each end. The wires connnecting the batteries to the electronics run along the inside of the capsule and are not visible.

by using three mutually orthogonal omniwheels to generate rotation about arbitrary axes. The SAMM is mounted as the end-effector on a Yaskawa Motoman MH5 6-DOF robotic manipulator. We chose our workspace to span between 75–200 mm from the center of the permanent magnet to ensure a high signal-to-noise ratio. Its size is limited by a combination of the strength of the prototype SAMM's permanent magnet and the sensitivity of the Hall-effect sensors. Due the homothetic property of magnetic fields, if the SAMM's magnet radius were scaled by η the field measured at $\eta\mathbf{p}$ would be the same as that measured at $\mathbf{p}$ with the original magnet. Tested locations were normalized by the radius ρ of the SAMM magnet, which is 25.4 mm, to enable our results to generalize to other magnetic field sources. The effect of increasing the sensor's sensitivity is not as straightforward because of the exponential decrease in magnetic field magnitude with distance, but typically more sensitive sensors have a smaller range and thus less measurement noise. When using higher sensitivities, one should ensure the sensing range is large enough to accommodate the desired range of external field measurements when combined with offsets from the internal magnetic field.

To quantify the accuracy of the proposed localization method, the capsule was mounted with accuracy of 1.5 mm and 3° using the test fixture shown in Fig. 3(b). The SAMM was moved relative to the fixed position of the capsule along seven directions spread throughout an octant of the workspace as shown in Fig. 3(c). The distance $||\mathbf{p}_c||$ was varied between 4ρ to 8ρ. At each location, the SAMM's position was held constant and $\mathbf{m}_r$ was rotated about seven different rotation axes, for five complete rotations each, to characterize the convergence properties of the localization method. Ten trials were completed at each location for statistical analysis. To ensure the tests with a stationary capsule give comparable results to more clinically realistic scenarios, the capsule was also tested in a lightly lubricated clear acrylic tube where it was free to rotate (Fig. 3(a)). The SAMM's maximum rotation speed is 3 Hz; to ensure the capsule remained in the step-out regime, these tests were performed at $||\mathbf{p}_c|| = 7\rho$. Closer distances could be achievable using an electromagnetic dipole source such as an Omnimagnet [27] and localizing with rotation speeds of 20–30 Hz, or by constructing a faster SAMM.

B. Prototype Capsule

This method was designed to be used in conjunction with a magnetic capsule with Hall-effect sensors embedded. One of the major problems associated with internal magnetic sensors, if used in conjunction with magnetic propulsion, is their close proximity to the capsule's internal magnet, whose field may dominate the external field we are trying to sense. One option is to employ large-range sensors, but these typically have more noise associated with their measurements at the signals of interest. An alternative, which we first presented in [20], is to strategically surround the internal magnet with six one-axis sensors that have negligible biasing in the sensor measurements from the internal magnet's field. Assuming the capsule's internal magnet can be modeled using (1), there are positions where the magnetic field points in a single cardinal direction as illustrated by the dashed/dotted lines in Fig. 4(a). By using a one-axis Hall-effect sensor, which measures the field component orthogonal to its surface and ignores all other field components, it is possible to place the sensor such that the internal magnet's field is parallel to the sensor's surface and provides negligible interference in its measurements. For example, the sensors measuring the field component in the $\mathbf{z}_c$ direction are placed at locations

where the field vector lies solely in the $\mathbf{x}_c - \mathbf{y}_c$ plane. These positions, denoted by dashed red lines in Fig. 4(a), lie along a line drawn out from the middle of the magnet at an angle of approximately 55° measured from $\mathbf{m}_c$. The $\mathbf{b_x}$ and $\mathbf{b_y}$ sensors are placed in regions parallel and perpendicular to $\mathbf{m}_c$, denoted by black dotted lines in Fig. 4(a). Using this strategy, we placed six sensors, one on each side of a cube, to provide two sensors in each of the three cardinal axes. As a cubic magnet is not perfectly modeled by (1) in the region where the sensors are placed, our final sensor positions were confirmed using finite-element-analysis software. The final sensor layout is illustrated in Fig. 4(b) and was chosen to be as close as possible to the ideal while still being feasible within our hardware constraints.

The sensor array was created using six printed circuit boards (Fig. 4(c)); on each was placed a one-axis Allegro A1392 linear Hall-effect sensor with a range of ±62 mT and a sensitivity of 25 V/T. The boards were mounted directly to the 108 mm^3 cubic NdFeB Grade N52 magnet in the layout shown in Fig. 4(b). Using our sensor configuration, the maximum offset from the internal magnet is 8.2 mT, which is measured by a $\mathbf{b_y}$ sensor. The average field offset across all six sensors is 2.9 mT. This is a significant improvement over the naive alternative of placing the $\mathbf{b_z}$ sensor along the $\mathbf{z}_c$-axis at 4.0 mm, similar to the $\mathbf{b_x}$ and $\mathbf{b_y}$ sensors; the field from the capsule's magnet at this position was measured by a Hirst GM08 gaussmeter as approximately 300 mT, which would saturate the sensor and make it useless. The small constant biases can be subtracted in software because the sensors remain fixed relative to the internal magnet.

The four-layer circular board (Fig. 4(d)) contains all the components to wirelessly transmit the six sensor readings to a computer. A Texas Instruments CC2530 microcontroller (MCU) was chosen for its low-power consumption and its internal transceiver. The MCU uses an interrupt-based approach to transition between the capsule's states and execute functions that require constant timing intervals. During a test, the sensors are read every 10 ms, but are sent wirelessly in batches of five readings per sensor at 20 Hz back to the computer. Before transmission, the measurements are timestamped on the MCU. The MCU and PC clocks are synchronized to ensure each $\mathbf{m}_r$ is correctly attributed to its corresponding sensor measurements by sending a flag to the MCU to start its timers at a known PC time. Two 1.55 V silver-oxide Energizer 386/301 watch batteries were used to power the capsule, which typically last one hour. The batteries and electronics were incorporated into a 3D-printed capsule as shown in Fig. 4(e).

The capsule used here (Fig. 4(e)) is a scaled down version of the one first presented in [20]. It is approximately 1.4 times the length of commercial capsule endoscopes and 1.2 times the width, with a length of 42 mm and diameter of 13.5 mm, not including a 1 mm helical thread used for propulsion. For comparison, Fig. 4(e) shows our capsule with Given Imaging's colon capsule along with a U.S. quarter. The size is constrained by the batteries. With these components a 1.2-scaled capsule was originally designed, but our batteries' steel casings became magnetized in the rotating field and created an unmodeled disturbance resulting in poor pose estimation. As a result, we lengthened our capsule slightly to mitigate this problem. In the future, custom non-magnetic batteries could be utilized; commercial low-magnetic batteries do not meet both our size and power constraints [28].

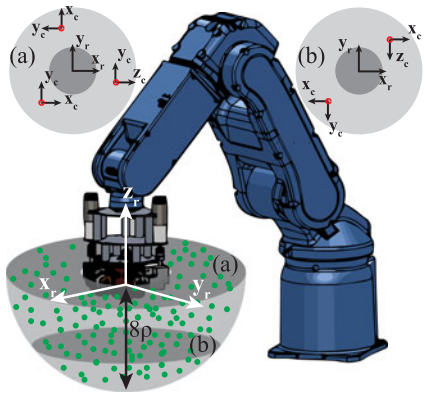

Fig. 5. Assuming the origin is located at the center of the external magnetic source, the workspace is restricted to a hemisphere in the negative $\mathbf{z}_r$ direction. Poses were randomly generated across the workspace, depicted by dots. The five initial states corresponding to the bottom rows of Table II are depicted in planes (a) and (b).

C. Sensor Calibration

Assuming the magnitude of the SAMM's dipole and each sensor's position offset is known, the sensitivities and orientations of the sensors were estimated using a constrained nonlinear least-squares algorithm to ensure accurate measurements. The sensor array was placed in the rigid test fixture (Fig. 3(b)) and the SAMM was moved relative to the capsule in a grid pattern (60 (w) × 60 (d) × 20 (h) mm^3) in 10 mm step increments, with the center of the grid 110 mm above the capsule; $\mathbf{m}_r$ was fixed throughout the test. A single dataset combined from two trials with dipole orientations of $[0\ 0\ 1]^T$ and $[0\ 0.707\ 0.707]^T$ was used. The sensitivity and orientation of each of the six sensors was solved simultaneously by estimating the readings using (2) and comparing them to the sensor measurements using the cost function $e = ||\mathbb{V}_m - \mathbb{V}_e||^2$. The comparisons were done in terms of the voltage output of the sensor because the sensitivity constant (α) that converts volts to mT was unknown. $\mathbb{V}_m$ is an array of voltage readings from the six sensors, and $\mathbb{V}_e = \mathbb{B}_e\alpha$. A total of 24 parameters were estimated: the fixed 6-DOF pose of the capsule, and three parameters for each of the sensors (the 2-DOF pointing orientation $\mathbf{s}$, and the scalar sensitivity α).

To evaluate the results of our sensor calibration, we compared the localization results using both the original nominal sensor values and the calibrated values across 210 tests with $||\mathbf{p}_c||$ spread evenly between 4ρ, 6ρ, and 7ρ. The nominal values (before calibration) resulted in a mean error of 4.9 mm and 7.8°, and a maximum error of 10.0 mm and 12.6°. The mean error using the calibrated values was reduced to 4.1 mm and 3.0° with the maximum error reduced to 8.6 mm and 6.2°.

IV. Characterization Using Simulations

Initial testing of the localization method was performed with a MATLAB simulation based on our experimental hardware, as depicted in Fig. 5. The origin of the SAMM's magnet was centered on the top surface of the workspace, whose plane lies orthogonal to the $\mathbf{z}_r$ axis. A spherical workspace was chosen to

TABLE I
COMPONENTS WHERE NOISE AND UNCERTAINTY WERE ADDED TO IMITATE EXPERIMENTALLY MEASURED RESULTS

Source of error	range
Sensor noise	± 0.114 mT
Time difference between sensor and dipole readings	± 2 ms
Capsule position uncertainty	1.5 mm
Capsule orientation uncertainty	3°
Dipole position uncertainty	0.5 mm
Dipole orientation uncertainty	2.4°
Dipole magnitude uncertainty	$\pm 5\%$

test positions uniformly; it can be reduced to a hemisphere in our application of capsule endoscopy because the capsule will reside in the human body, whose local tangent plane can be drawn to cut the spherical workspace in half. Due to hardware constraints, the capsule cannot be closer than 3ρ to the center of the SAMM's magnet, so the hemisphere shape is further reduced to a spherical shell that spans from 3ρ to 8ρ as shown in Fig. 5. Each of the tested 6-DOF poses were randomly generated from the workspace.

In ideal conditions, if no noise or uncertainty is modeled, the algorithm estimates the capsule's pose with only rounding error in both the position (4.6×10^{-14} mm) and orientation (3.4×10^{-14} °), across 100 random poses. However, the sensor array and the dipole field have uncertainties, and signals are noisy, so a more realistic simulation was conducted where noise and uncertainties were added. These sources, which were derived from our experimental hardware, are listed along with their ranges in Table I. Note the sensor noise remains constant, so as $||\mathbf{p}_c||$ increases, the magnitude of the external field and the signal-to-noise ratio decrease, resulting in worse localization. The position and orientation uncertainty, both for the capsule and dipole source, stem from how accurately our ground truth is known. The time difference is a result of our time resolution. Including the noise and uncertainty resulted in an error of 2.2 ± 0.8 mm and $1.7° \pm 0.9°$ across 100 random poses (throughout this paper all errors are reported as the mean $\pm$ standard deviation). The orientation error is in terms of the angle-axis representation.

A known limitation of iterative methods is their dependence on the initial condition; if it is not in close proximity to the global minimum (the true capsule pose) the method may converge to a local minimum and result in poor localization. We do not assume prior knowledge of the capsule's pose, so the initial guess was chosen directly below the SAMM centered vertically in the hemispherical workspace with an orientation matching the external magnetic source's frame. Across 1,000 random poses, 98.7% resulted in a average error of 2.3 ± 1.0 mm and $1.8° \pm 0.8°$. The remaining 1.3% converged to an incorrect local minimum, typically, a pose that mirrors the true capsule pose. To ensure safety, we desire an algorithm that always converges to the global minimum.

One option to overcome the problem of local minimums is using an additional algorithm to estimate an initial condition that will be in close proximity to the optimal pose [10], and our previous non-iterative algorithm could be used to provide an initial guess [18]. Another option is to choose multiple initial conditions spread throughout the workspace and select the one that results in the minimum norm in the residual error between the sensor measurements and their estimates. Because we have a known workspace, if the algorithm converges to a position outside of the workspace (e.g., $\mathbf{p}_c$ has a positive $\mathbf{z}$ component) it is not considered a failure; instead, the initial conditions are modified by adding randomly generated noise from a uniform distribution on the interval ± 70 mm to each position component and a rotation on the interval of $\pm 45°$ about a random axis and the algorithm is run again. If the algorithm converges to a position inside the workspace that is not within 10 mm of the true capsule pose, it is considered a failure. We found using five structured initial conditions was sufficient for 100% convergence across 10,000 random poses. The five initial conditions are split across two planes in the hemispherical workspace as shown in Fig. 5. Other tested initial configurations along with their convergence rate to the true capsule pose are shown in Table II. Converging outside of the workspace is extremely rare, it occurs less than 0.5% of the time, when using five initial conditions. If a larger workspace is used, additional initial states may be necessary.

TABLE II
PERCENT CONVERGENCE TO TRUE CAPSULE POSE USING VARIOUS INITIAL STATES WITH POSITION VECTOR $\mathbf{p}_c$ IN MM AND ORIENTATION ANGLE-AXIS $\mathbf{k}$ IN RAD

Initial State $\mathbf{p}_c$	Initial State $\mathbf{k}$	Tested poses	Convergence
$[0\ 0\ -140]^T$	$[0\ 0\ 0]^T$	1000	98.7%
$[-81\ -81\ -81]^T$	$[0\ 0\ 0]^T$	1000	99.4%
$[81\ 81\ -81]^T$	$[0\ 0\ \frac{\pi}{2}]^T$		
$[-81\ -81\ -81]^T$	$[0\ 0\ 0]^T$	1000	99.8%
$[110\ -30\ -81]^T$	$[\frac{\pi}{2}\ 0\ 0]^T$		
$[-30\ 110\ -81]^T$	$[0\ \frac{\pi}{2}\ 0]^T$		
$[-81\ -81\ -81]^T$	$[0\ 0\ 0]^T$	10000	99.9%
$[110\ -30\ -81]^T$	$[\frac{\pi}{2}\ 0\ 0]^T$		
$[-30\ 110\ -81]^T$	$[0\ \frac{\pi}{2}\ 0]^T$		
$[0\ 0\ -140]^T$	$[0\ 0\ \frac{\pi}{2}]^T$		
$[-99\ -99\ 0]^T$	$[0\ 0\ 0]^T$	10000	100%
$[135\ -36\ 0]^T$	$[0\ \frac{\pi}{2}\ 0]^T$		
$[-36\ 135\ 0]^T$	$[0\ 0\ \frac{\pi}{2}]^T$		
$[-81\ -81\ -81]^T$	$[0\ 0\ \pi]^T$		
$[81\ 81\ -81]^T$	$[\frac{\pi}{2}\ 0\ 0]^T$		

If there is prior knowledge of the capsule's pose, using a single initial condition that is within 5 cm and 90° was sufficient to converge to the capsule's true pose every time over 10,000 randomly chosen poses. When used for capsule endoscopy, the initial localization will have no prior information about the capsule, but for subsequent tracking, the position of the capsule will generally be in close proximity to the previous position. However, prior knowledge of the capsule's orientation will be much less certain, particularly considering the use of rotating fields. By reducing the bounds on the position to 3 cm, the orientation constraints could be relaxed to 180° and still converge to the true pose in 99.9% of cases across 10,000 randomly chosen poses.

V. EXPERIMENTAL RESULTS AND DISCUSSION

When localizing the capsule, there is a trade-off between accuracy and the time to collect the sensor data. Fig. 6 compares

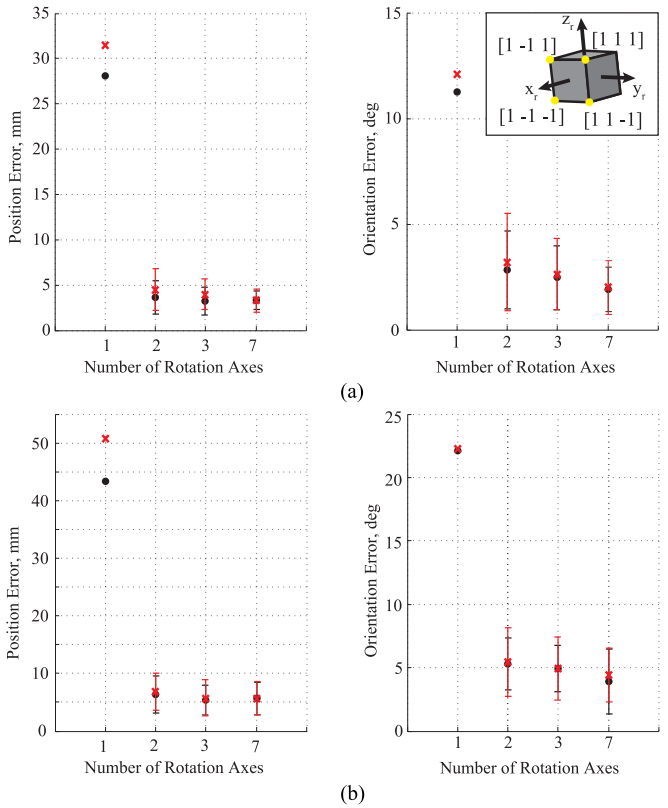

Fig. 6. Comparison of the effect of the angular velocity of the applied field and number of rotation axes on the accuracy of the localization. Data is represented as mean ± standard deviation over 70 trials for 2 Hz (black dot) and 3 Hz (red x). The standard deviation for one axis was too large to show graphically. (a) shows the results from a capsule rigidly mounted at 6ρ, and (b) show results for a capsule in step-out at 7ρ. The inset depicts the additional four axes used when testing seven rotation axes.

the average and standard deviation in error across different rotation speeds $||\boldsymbol{\Omega}||$ and number of rotation axes. Intuitively, the rotation speed of the dipole field should not substantially influence the accuracy of the localization if both data sets use the same number of complete dipole rotations and are below the Nyquist frequency such that no aliasing has occurred; our tests confirm this. The data sets in Fig. 6 each include 10 trials from seven positions, for a total of 70 trials. There is no appreciable difference between $||\boldsymbol{\Omega}|| = 2$ Hz or 3 Hz. Larger $||\boldsymbol{\Omega}||$ are recommended because the time required to collect the localization data is reduced.

Fig. 6 also shows the error when rotating the dipole field about one, two, three, or seven distinct rotation axes. One full rotation of data is collected about each axis. For one axis, Fig. 6 combines the data from all three coordinate axes $(\mathbf{x}_r, \mathbf{y}_r, \mathbf{z}_r)$ considered individually, and for two axes Fig. 6 combines the data across the three possible combinations of axes ($\mathbf{x}_r$ and $\mathbf{y}_r$, $\mathbf{x}_r$ and $\mathbf{z}_r$, $\mathbf{y}_r$ and $\mathbf{z}_r$) considered individually. The additional four axes chosen when rotating about seven axes are shown in the inset of Fig. 6. Rotating about two axes provides a significant advantage over one; an increasingly diminishing return in accuracy results when adding additional rotation axes. When the capsule is rigidly mounted (Fig. 6(a)), there is a 12% reduction in position error when using three axes instead of two; the error

TABLE III
COMPARISON OF ERROR (MEAN ± STANDARD DEVIATION OVER 70 TRIALS) FOR ONE AND FIVE ROTATIONS ABOUT $\mathbf{x}_r$, $\mathbf{y}_r$, AND $\mathbf{z}_r$

	Rotations	
Pose	1	5
Rigid, 6ρ	4.0 ± 1.7 mm, $2.6 \pm 1.2°$	3.9 ± 1.7 mm, $2.6 \pm 1.2°$
Step-out, 7ρ	5.7 ± 3.0 mm, $4.9 \pm 2.4°$	5.6 ± 2.9 mm, $4.7 \pm 2.4°$

TABLE IV
POSITION (MM) AND ORIENTATION ERROR (MEAN ± STANDARD DEVIATION OVER 10 TRIALS) OF CAPSULES RIGIDLY MOUNTED (4ρ TO 8ρ) AND IN STEP-OUT (7ρ). DATA COLLECTED BY ROTATING THE EXTERNAL FIELD ONCE AROUND EACH OF THREE ORTHOGONAL AXES AT 3 HZ. SEE FIG. 3(C) FOR LOCATION DEFINITIONS

Rigid?	Y	Y	Y	N	Y
Location	4ρ	6ρ	7ρ	7ρ	8ρ
001	2.8 ± 0.4	2.8 ± 0.7	4.9 ± 1.3	4.5 ± 1.6	4.0 ± 1.0
	$2.7° \pm 0.6°$	$3.4° \pm 0.8°$	$2.4° \pm 0.8°$	$4.3° \pm 0.8°$	$2.9° \pm 1.0°$
011	4.2 ± 2.0	4.1 ± 1.6	5.6 ± 1.9	4.9 ± 1.7	8.1 ± 3.4
	$2.8° \pm 1.9°$	$1.7° \pm 0.3°$	$2.1° \pm 0.8°$	$6.6° \pm 2.0°$	$2.4° \pm 1.2°$
111	4.0 ± 0.9	3.4 ± 1.4	5.5 ± 1.8	11.5 ± 1.8	4.6 ± 2.4
	$4.2° \pm 0.3°$	$2.1° \pm 0.9°$	$4.0° \pm 0.9°$	$6.3° \pm 1.0°$	$2.0° \pm 1.0°$
101	3.6 ± 1.0	5.9 ± 1.4	6.1 ± 0.8	6.8 ± 2.3	7.6 ± 2.5
	$3.5° \pm 0.7°$	$1.9° \pm 0.6°$	$3.0° \pm 0.6°$	$6.3° \pm 1.0°$	$2.8° \pm 1.3°$
100	2.8 ± 1.2	4.9 ± 1.6	4.7 ± 2.5	3.5 ± 1.6	11.7 ± 3.8
	$3.4° \pm 0.6°$	$2.9° \pm 0.8°$	$3.1° \pm 0.7°$	$1.6° \pm 0.9°$	$4.6° \pm 1.4°$
110	3.5 ± 0.6	4.3 ± 0.9	6.8 ± 1.4	4.5 ± 1.4	7.0 ± 1.3
	$1.8° \pm 0.4°$	$1.7° \pm 0.4°$	$2.0° \pm 1.4°$	$7.2° \pm 0.3°$	$2.1° \pm 0.8°$
010	2.3 ± 0.6	2.4 ± 1.2	3.5 ± 1.3	3.9 ± 1.0	3.1 ± 0.9
	$5.5° \pm 0.6°$	$4.8° \pm 0.4°$	$3.5° \pm 0.9°$	$1.9° \pm 1.0°$	$3.4° \pm 0.5°$

is reduced an additional 8% between three and seven axes, but the time to collect the data more than doubles. A capsule in the step-out regime (Fig. 6(b)) has a larger disparity, with a 15% reduction in position error between two and three axes and less than 1% additional reduction when increasing to seven axes. For the remainder of this paper we chose to rotate about the *three* robot-frame coordinate axes as it provides a good balance between speed and accuracy. For more time-sensitive applications, rotating the external field about a set of any two orthogonal axes will provide similar results.

Next, we tested whether collecting more data about each of the three rotation axes $(\mathbf{x}_r, \mathbf{y}_r, \mathbf{z}_r)$ would provide a more accurate pose estimate. Table III shows that using more than one rotation about each of the three orthogonal axes leads to negligible improvement in accuracy. This is true both when the capsule is held stationary and when it is free to rotate in the step-out regime.

Table IV shows the localization error with distances varying from 4ρ to 8ρ, which in our setup is approximately 100–200 mm. All reported errors used one rotation of the dipole field at 3 Hz about each of the three robot-frame coordinate axes. As expected, the error increases as the distance increases. In our setup, there are six signal-to-noise ratios, one for each sensor, at 8ρ all have fallen below 10:1. This results in large increases to the variance of the position errors in certain directions (011, 111, 101, 100; see Fig. 3(c)), which implies these regions are more sensitive to noise and uncertainty. Actuating and localizing near

the "radial" positions of (001, 010) is recommended because these have the lowest mean error, and the control authority of the desired rotation axis is the most robust to localization errors [29]. According to the simulation, the algorithm should perform equally well across the entire workspace; the differences we see experimentally across locations are likely due to environmental factors such as unmodeled magnetic disturbances.

For comparison, results from both a rigidly fixed capsule and one that was free to rotate during the test are provided in Table IV for 7ρ. The position error when the capsule is free to rotate is comparable to that when it is held rigid. This is expected as the field is rotating above the step-out frequency such that the capsule has little net motion in these tests. The notable exception is in direction 111. It is unclear why this location performs consistently worse in the step-out regime than when rigidly fixed. The rigidly held capsules, which do not rely on battery power, give the best-case results. In an attempt to further isolate the batteries from the sensor array by lengthening the capsule by 4 mm, the error at 111 was cut almost in half, to 6.4 ± 1.0 mm. The remaining locations are already consistent with the rigidly fixed capsules.

The orientation error reported in Table IV is half of what we reported in our preliminary presentation of this method [19]. Subsequent to that publication, we performed additional calibration on the sensor array and SAMM device and were able to more accurately estimate the capsule's orientation during testing. As expected, the orientation error of the capsule in step-out is worse than when rigidly held because its orientation is not as accurately known and it changes slightly throughout the data collection as it wiggles back and forth in the rotating field.

VI. Demonstration of Capsule Propulsion

A proof-of-concept propulsion system was designed that utilizes the estimated pose from our localization method to propel a magnetic capsule through both straight and curved lumens using a single rotating dipole source for both propulsion and localization. Although in the current form these are decoupled such that the capsule's movement is periodically paused to re-localize, this provides the first step toward utilizing rotating magnetic fields in a more clinically realistic fashion. The demonstrations confirm that our localization method provides sufficient accuracy for propulsion using rotating dipole fields; all prior work from our group relied on cameras for position feedback [6].

From [30], if a dipole source is rotated about an axis $\hat{\mathbf{\Omega}}$, such that its magnetic moment is always orthogonal to the rotation axis, the applied field at any position in space rotates orthogonal to some constant axis $\hat{\boldsymbol{\omega}}_c$. Assuming a screw-type capsule is constrained to a lumen, at the capsule's position, we desire $\hat{\boldsymbol{\omega}}_c$ to be aligned with the lumen (and the capsule's principle axis $\mathbf{x}_c$) to provide a useful magnetic torque. Given the capsule's pose from our localization method, we calculate the actuator magnet's desired rotation axis, from [6]:

$$\hat{\mathbf{\Omega}} = \widehat{\mathbf{B}\hat{\boldsymbol{\omega}}_c} \tag{4}$$

where $\mathbf{B}$ is from (1). Prior to propulsion the capsule must be localized. We assume the capsule is placed within our known workspace (in capsule endoscopy this would be the abdomen); no additional information about the pose is required. In our experimental demonstrations, the SAMM was started in an arbitrary position above the approximate center of the workspace. The first localization used five initial guesses as described in Section IV. For the remainder of the trajectory, the previously estimated pose was used as the initial condition for the iterative algorithm. During the propulsion phase, we assume the capsule's position and heading remain constant. Prior to collecting a batch of localization data, the SAMM was raised 50 mm in the vertical direction to ensure the capsule would be in the step-out regime. This additional movement of the SAMM is not necessary for our algorithm; it was required due to our hardware's limited $||\mathbf{\Omega}||$. Approximately one rotation about each of the $\mathbf{x}_r$, $\mathbf{y}_r$, and $\mathbf{z}_r$ axes in the SAMM's coordinate frame was collected. After each localization, the SAMM's pose was updated based on the capsule's estimated state before resuming propulsion. A block diagram of the propulsion system is depicted in Fig. 7.

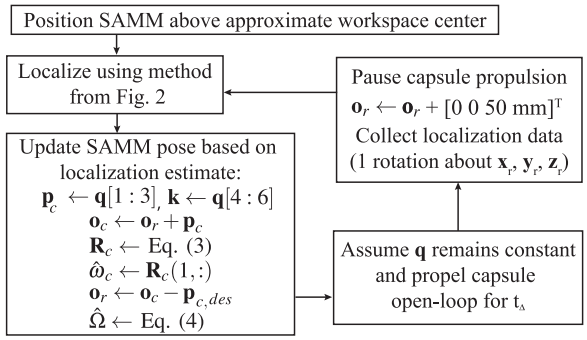

Fig. 7. A block diagram of the system used to propel the capsule through the two lumen trajectories. $\mathbf{q}$ is the capsule's state, $\hat{\boldsymbol{\omega}}$ is the SAMM's desired rotation axis, $\hat{\boldsymbol{\omega}}_c$ is the heading of the capsule, $\mathbf{p}_{c,\,des}$ is the desired position of the capsule ($\mathbf{o}_c$) relative to the SAMM ($\mathbf{o}_r$) for propulsion, and t_Δ is the time interval between localizations. Note $\mathbf{p}_{c,\,des}$ may be user-specified or the result of an optimization routine.

When propelling the capsule through the straight lumen (Fig. 8(a)), a configuration where the external magnet leads the capsule was chosen because in these positions the attractive magnetic force combines with the magnetic torque to result in faster capsule propulsion than in "radial" positions [6]. It took two minutes for the capsule to traverse the straight path with an average forward velocity of 2.1 mm/s. Using the same propulsion system, the capsule was also propelled through a semicircular trajectory shown by the composite image in Fig. 8(b). For this path, an arbitrary relative position was chosen to ensure our method can be generalized to any position. It took approximately 6.5 minutes to complete the trajectory, with an average speed of 1.4 mm/s. It should be noted that neither the actuation configuration and parameters during the propulsion phase nor the time between localizations have been optimized in these demonstrations so it should not be assumed that we have achieved maximum average speed. Additionally, the plastic tubing does not accurately model intestine properties so these velocities should not be assumed to be clinically realistic.

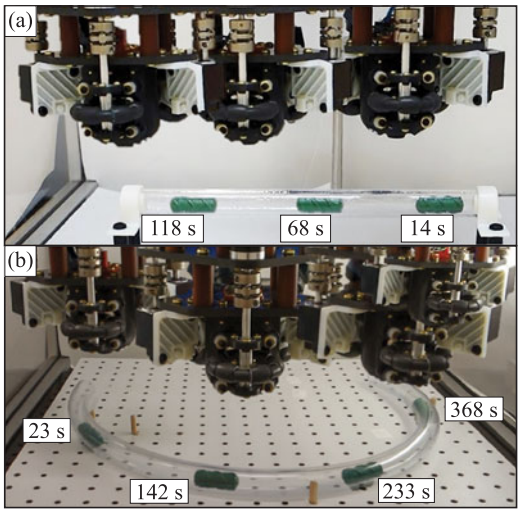

Fig. 8. Experimental demonstration of capsule propulsion using the system described in Fig. 7. (a) The SAMM was placed in a leading configuration with $\mathbf{p}_{c,\,des} = [0\ 58\ -100]^T$ mm and $||\mathbf{\Omega}|| = 0.5$ Hz during propulsion. (b) The SAMM was placed in an arbitrary configuration with $\mathbf{p}_{c,\,des}$ a function of the capsule's heading such that the SAMM's relative placement to the capsule remains constant regardless of the capsule's heading with $||\mathbf{p}_{c,\,des}|| = 100$ mm and $||\mathbf{\Omega}|| = 0.5$ Hz during propulsion. The capsule's propulsion was periodically paused for localization with $t_\Delta = 12$ sec in (a) and $t_\Delta = 15$ sec in (b). Please see supplementary video.

VII. Conclusion

We have described and characterized a magnetic-localization method that enables a screw-type magnetic capsule, equipped with an embedded permanent magnet and Hall-effect sensors, to be localized using a rotating magnetic-dipole field. We showed the localization method provided accurate pose estimation to within a few millimeters in position and a few degrees in orientation throughout a usable workspace. This localization method was developed as a complement to methods previously developed to propel a screw-type magnetic capsule using a single rotating magnetic dipole. We experimentally demonstrated that the localization is sufficiently accurate to enable the use of our propulsion method with no other form of localization. The target application of this technology is active capsule endoscopy of the small intestines, with potential for use in the colon as well.

References

[1] P. R. Slawinski, K. L. Obstein, and P. Valdastri, "Emerging issues and future developments in capsule endoscopy, " *Techn. Gastrointestinal Endo*, vol. 17, no. 1, pp. 40–46, 2015.

[2] Z. Liao *et al.*, "Feasibility and safety of magnetic-controlled capsule endoscopy system in examination of human stomach: A pilot study in healthy volunteers, " *J. Interventional Gastroenterol.*, vol. 2, no. 4, pp. 155–160, 2012.

[3] X. Wang and M.-H. Meng, "Computational aspects in actuation and guidance mechanism for wireless active capsule endoscope, " in *Proc. IEEE Int. Conf. Intel. Robots Syst.*, 2008, pp. 1198–1203.

[4] G. Ciuti, P. Valdastri, A. Menciassi, and P. Dario, "Robotic magnetic steering and locomotion of capsule endoscope for diagnostic and surgical endoluminal procedures, " *Robotica*, vol. 28, pp. 199–207, 2010.

[5] F. Carpi, N. Kastelein, M. Talcott, and C. Pappone, "Magnetically controllable gastrointestinal steering of video capsules, " *IEEE Trans. Biomed. Eng.*, vol. 58, no. 2, pp. 231–234, Feb. 2011.

[6] A. W. Mahoney and J. J. Abbott, "Generating rotating magnetic fields with a single permanent magnet for propulsion of untethered magnetic devices in a lumen, " *IEEE Trans. Robot.*, vol. 30, no. 2, pp. 411–420, Apr. 2014.

[7] J. Kim, Y. Kwon, and Y. Hong, "Automated alignment of rotating magnetic field for inducing a continuous spiral motion on a capsule endoscope with a twistable thread mechanism, " *Int. J. Precision Eng. Manuf.*, vol. 13, no. 3, pp. 371–377, 2012.

[8] S. Song *et al.*, "6-d magnetic localization and orientation method for an annular magnet based on a closed-form analytical model, " *IEEE Trans. Mag.*, vol. 50, no. 9, Sep. 2014, Art. no. 5000411.

[9] D. M. Pham and S. Aziz, "A real-time localization system for an endoscopic capsule, " in *Proc. IEEE 9th Int. Conf. Intell. Sens., Sens. Netw. Inf. Process.*, 2014, pp. 1–6.

[10] C. Hu, M. Li, S. Song, W. Yang, R. Zhang, and M. Q.-H. Meng, "A cubic 3-axis magnetic sensor array for wirelessly tracking magnet position and orientation, " *IEEE Sensors J.*, vol. 10, no. 5, pp. 903–913, May 2010.

[11] W. Weitschies, H. Blume, and H. Monnikes, "Magnetic marker monitoring: High resolution real-time tracking of oral solid dosage forms in the gastrointestinal tract, " *Eur. J. Pharmaceutics Biopharmaceutics*, vol. 74, no. 1, pp. 93–101, 2010.

[12] M. Salerno, F. Mulana, R. Rizzo, A. Landi, and A. Menciassi, "Magnetic and inertial sensor fusion for the localization of endoluminal diagnostic devices, " *Int. J. Comput. Assisted Radiol. Surgery*, vol. 7, no. S1, pp. 229–235, 2012.

[13] C. D. Natali, M. Beccani, N. Simaan, and P. Valdastri, "Jacobian-based iterative method for magnetic localization in robotic capsule endoscopy, " *IEEE Trans. Robot.*, vol. 32, no. 2, pp. 327–338, Apr. 2016.

[14] M. Kim, Y. Hong, and E. Lim, "Position and orientation detection of capsule endoscopes in spiral motion, " *Int. J. Precision Eng. Manuf.*, vol. 11, no. 1, pp. 31–37, 2010.

[15] M. Salerno *et al.*, "A discrete-time localization method for capsule endoscopy based on on-board magnetic sensing, " *Meas. Sci. Technol.*, vol. 23, no. 1, 2012, Art. no. 015701.

[16] D. Son, S. Yim, and M. Sitti, "A 5-d localization method for a magnetically manipulated untethered robot using a 2-d array of hall-effect sensors, " *IEEE/ASME Trans. Mechatronics*, vol. 21, no. 2, pp. 708–716, Apr. 2016.

[17] S. Yim and M. Sitti, "3-d localization method for a magnetically actuated soft capsule endoscope and its applications, " *IEEE Trans. Robot.*, vol. 29, no. 5, pp. 1139–1151, Oct. 2013.

[18] K. M. Popek, A. W. Mahoney, and J. J. Abbott, "Localization method for a magnetic capsule endoscope propelled by a rotating magnetic dipole field, " in *Proc. IEEE Int. Conf. Robot. Autom.*, 2013, pp. 5328–5333.

[19] K. M. Popek and J. J. Abbott, "6-d localization of a magnetic capsule endoscope using a stationary rotating magnetic dipole field, " in *Proc. Hamlyn Symp. Med. Robot.*, 2015, pp. 47–48.

[20] K. M. Miller, A. W. Mahoney, T. Schmid, and J. J. Abbott, "Proprioceptive magnetic-field sensing for closed-loop control of magnetic capsule endoscopes, " in *Proc. IEEE Int. Conf. Intel. Robots Syst.*, 2012, pp. 1994–1999.

[21] E. P. Furlani, *Permanent Magnet and Electromechanical Devices: Materials, Analysis, and Applications*, 1st ed. San Diego, CA, USA: Academic Press, 2001.

[22] A. J. Petruska and J. J. Abbott, "Optimal permanent-magnet geometries for dipole field approximation, " *IEEE Trans. Mag.*, vol. 49, no. 2, pp. 811–819, Feb. 2013.

[23] R. M. Murray, Z. Li, and S. S. Sastry, *A Mathematical Introduction to Robotic Manipulation*. Boca Raton, FL, USA: CRC Press, 1994.

[24] J. Nocedal and S. J. Wright, *Numerical Optimization*, 2nd ed.New York, NY, USA: Springer, 2006.

[25] G. Guennebaud *et al.*, "Eigen v3, " 2010. [Online]. Available: http://eigen.tuxfamily.org

[26] S. E. Wright, A. W. Mahoney, K. M. Popek, and J. J. Abbott, "A spherical-magnet end-effector for robotic magnetic manipulation, " in *Proc. IEEE Int. Conf. Robot. Autom.*, 2015, pp. 1190–1195.

[27] A. J. Petruska and J. J. Abbott, "Omnimagnet: An omnidirectional electromagnet for controlled dipole-field generation, " *IEEE Trans. Magn.*, vol. 50, no. 7, Jul. 2014, Art. no. 8400810.

[28] *CR1130*, Powerstream. 2016. [Online]. Available: http://www.powerstream.com

[29] A. W. Mahoney and J. J. Abbott, "Control of untethered magnetically actuated tools with localization uncertainty using a rotating permanent magnet, " in *Proc. IEEE Int. Conf. Biomed. Robot. Biomechatronics*, 2012, pp. 1632–1637.

[30] E. Paperno, I. Sasada, and E. Leonovich, "A new method for magnetic position and orientation tracking, " *IEEE Trans. Magn.*, vol. 37, no. 4, pp. 1938–1940, Aug. 2001.